Hydrol. Earth Syst. Sci. Discuss., 12, 12247–12280, 2015
www.hydrol-earth-syst-sci-discuss.net/12/12247/2015/
doi:10.5194/hessd-12-12247-2015

Hydrology and Earth System Sciences
Open Access
Discussions

Technical Note: Three-dimensional transient groundwater flow due to localized recharge with an arbitrary transient rate in unconfined aquifers

C.-H. Chang, C.-S. Huang, and H.-D. Yeh

Institute of Environmental Engineering, National Chiao Tung University, Hsinchu, Taiwan

Received: 18 September 2015 – Accepted: 31 October 2015 – Published: 24 November 2015

Correspondence to: H.-D. Yeh (hdyeh@mail.nctu.edu.tw)

Published by Copernicus Publications on behalf of the European Geosciences Union.

Abstract

Most previous solutions for groundwater flow induced by localized recharge assumed either aquifer incompressibility or two-dimensional flow in the absence of the vertical flow. This paper develops a new three-dimensional flow model for hydraulic head variation due to localized recharge in a rectangular unconfined aquifer with four boundaries under the Robin condition. A governing equation for describing the head distribution is employed. The first-order free surface equation with a source term defining a constant recharge rate over a rectangular area is used to depict water table movement. The solution of the model for the head distribution is developed by the methods of the Laplace transform and double integral transform. Based on the convolution technique, the present solution is applicable to flow problems accounting for arbitrary time-depending recharge rates. The solution of depth-average head can then be obtained by integrating the head solution to depth and dividing the result by the aquifer thickness. The use of rectangular aquifer domain has two merits. One is that the integration for estimating the depth-average head can be analytically achieved. The other is that existing solutions based on aquifers of infinite extent can be considered as special cases of the present solution before the time having the aquifer boundary effect on the head distribution. With the help of the present solution, the assumption of neglecting the vertical flow effect on the transient head at an observation well outside a recharge region can be assessed by a dimensionless parameter related to the aquifer horizontal and vertical hydraulic conductivities, initial aquifer thickness, and a shortest distance between the observation well and the edge of the recharge region. The validity of assuming aquifer incompressibility is dominated by the ratio of the aquifer specific yield to its storage coefficient. In addition, the sensitivity analysis is performed to investigate the head response to the change in each of the aquifer parameters.

HESSD

12, 12247–12280, 2015

1 Introduction

Water table rises due to localized recharge such as rainfall, lakes, and agricultural irrigation into the regional area of the aquifer. Excess recharge may cause soil liquefaction or wet basements of buildings. Groundwater flow behavior induced by recharge into aquifers is therefore crucial in water resource management. The Boussinesq equation has been extendedly used to describe horizontal flow without the vertical component in unconfined aquifers (e.g., Ireson and Butler, 2013; van der Spek et al., 2013; Yeh and Chang, 2013; Chor and Dias, 2015; Hsieh et al., 2015; Liang and Zhang, 2015; Liang et al., 2015). The equation can be linearized on the basis of the assumption that time-varying saturated aquifer thickness is constant. The assumption is valid when the recharge rate is smaller than the hydraulic conductivity and/or the rise in the water table is smaller than the initial aquifer thickness. Marino (1967) presented quantitative criteria to validate the assumption, and the criteria are shown in the next section. On the basis of the assumption, analytical solutions of the linearized Boussinesq equation for various aquifer configurations were developed.

The rate of localized recharge can be a constant for a long term but should be dependent of time for a short term (Rai et al., 2006). An exponentially decaying function of time is usually used for recharge intensity decreasing from a certain rate to an ultimate one. An arbitrary time-depending recharge rate is commonly approximated as the combination of several linear segments of time to develop analytical solutions for water table rise subject to the recharge.

Analytical models accounting for water table rise in an aquifer near recharge region regarded as an infinite-length strip are reviewed. One-dimensional (1-D) flow perpendicular to the strip is considered while the flow along the strip is assumed ignorable. These models deal with aquifers of finite or infinite extent with various types of outer boundary conditions. Hantush (1963) considered an aquifer of infinite extent without a lateral boundary. Rao and Sarma (1980) considered an aquifer of finite extent with two constant-head (also called Dirichlet) boundaries. Later, they developed a solution

HESSD
12, 12247–12280, 2015

(Rao and Sarma, 1984) for a finite-extent aquifer between no-flow and constant-head boundaries. Latinopoulos (1986) deliberated on a finite-extent aquifer between two boundaries of a Robin boundary and the other one under either the Dirichlet or no-flow condition. The recharge is treated as a periodical pulse consisting of constant rates for rainy seasons and zero for dry seasons. Bansal and Das (2010) studied an aquifer extending semi-infinitely from a Dirichlet boundary and overlying a sloping impervious base and indicated that the change in groundwater mound induced by strip-shaped recharge increases with the base slope.

A variety of analytical models were presented to describe water table rise for two-dimensional (2-D) flow induced by rectangle-shaped recharge into unconfined aquifers. The differences between these solutions are addressed below. Hantush (1967) considered an infinite-extent aquifer with localized recharge having a constant rate. Manglik et al. (1997) handled an arbitrary time-varying rate of recharge into a rectangular aquifer bounded by no-flow stratum. Manglik and Rai (1998) investigated groundwater flow due to recharge with irregularly time-varying rates for a rectangular aquifer where the lateral boundary is under the Dirichlet condition. Chang and Yeh (2007) considered one localized recharge and multiple extraction wells in an anisotropic aquifer overlying an impervious sloping bed. They indicated that the aquifer anisotropy and bottom slope notably influence water table distributions. Bansal and Teloglou (2013) explored the problem of a groundwater mound subject to multiple localized recharges and withdrawal wells in an unconfined aquifer overlying a semi-permeable base. They indicated that groundwater mound rises as the decrease in the aquifer hydraulic conductivity.

Some articles discussed water table rise near circle-shaped recharge region and thus considered radial groundwater flow which is symmetric to the center of the recharge region. Rai et al. (1998) presented an analytical model describing water table growth subject to an exponentially decaying rate of recharge in a circle-shaped unconfined aquifer with an outer Dirichlet boundary. Illas et al. (2008) considered the same model, but the aquifer has leakage. They indicated that leakage across the aquifer bottom significantly influences spatiotemporal water table distributions despite a small

HESSD
12, 12247–12280, 2015

amount of the leakage. On the other hand, some researches considered radial and vertical flows adjacent to a circle-shaped recharge region in an infinite-extent unconfined aquifer. A first-order free surface equation as the top boundary condition of the aquifer is applied to describe water table rise. Zlotnik and Ledder (1992) developed analytical models for describing the distributions of hydraulic head and flow velocity due to constant-rate recharge. They found that models neglecting aquifer compressibility overestimate the head and flow velocity in the aquifer domain. Ostendorf et al. (2007) derived an analytical model for head distribution in an aquifer with considering an exponentially decaying rate of recharge. Predictions of their solution agreed well with the field data obtained in the Plymouth-Carver Aquifer in southeastern Massachusetts given by Hansen and Lapham (1992).

Some studies neglected aquifer compressibility to build a three-dimensional (3-D) flow model describing spatiotemporal head distributions in an unconfined aquifer with a rectangular region. Dagan (1967) derived an approximate solution of the model to make predictions for a small ratio of the recharge rate over the hydraulic conductivity. Zlotnik and Ledder (1993) presented an analytical model and found that groundwater flow are horizontal in the area beyond 150 % of the length or width of the recharge region.

It would be informative to summarize the above-mentioned models in Table 1. The solutions of the models are classified according to flow dimensions into 1-D, 2-D, and radial flows and further categorized according to aquifer domain, aquifer boundary conditions, recharge region, and recharge rate. The table shows that those solutions assume either no vertical flow or aquifer incompressibility. In addition, the Dirichlet and no-flow conditions considered by some of those solutions are not applicable to a boundary having a semi-permeable stratum, but the Robin condition is. The former two conditions are indeed special cases of the third one.

The objective of this paper is to develop a new mathematical model for depicting the spatiotemporal hydraulic head distributions subject to localized recharge with an arbitrary time-varying recharge rate in a rectangular-shaped unconfined aquifer. The

HESSD
12, 12247–12280, 2015

four boundaries are considered under the Robin condition which can reduce to the Dirichlet or no-flow condition. A governing equation describing 3-D transient flow subject to the effect of aquifer compressibility is used. A first-order free surface equation with a source term representing recharge rate is chosen to describe the top boundary condition. The transient head solution of the model is derived by the methods of Laplace transform, double-integral transform, and convolution theory. The sensitivity analysis based on the present solution is performed to study the head response to the change in each of hydraulic parameters. On the basis of solution's predictions, the effect of the Robin boundaries on time-depending head distributions at observation wells is investigated. A quantitative criterion under which the Robin condition reduces to the Dirichlet and no-flow ones is provided. In addition, quantitative criteria for the validity of two assumptions of aquifer incompressibility and no vertical flow are provided and errors arising from the assumptions in the hydraulic head are also discussed. Temporal head distributions accounting for transient recharge rates are demonstrated as well.

2 Methodology

2.1 Mathematical model

A mathematical model is developed for describing spatiotemporal hydraulic head distributions induced by localized recharge in a rectangular unconfined aquifer as illustrated in Fig. 1a. The four boundaries of the aquifer are considered under the Robin condition. The aquifer has the widths of l and w in x and y directions, respectively. The recharge uniformly distributes over a rectangular region having widths a and b in x and y directions, respectively. One of the location of the region corners is designated at (x_1,y_1). The shortest distance between the edge of the region and an observation well is d. The shortest distances measured from the edge of the region to boundaries 1, 2, 3 and 4 are denoted as d_1, d_2, d_3, and d_4, respectively. The initial aquifer thickness is B as shown in Fig. 1b.

HESSD
12, 12247–12280, 2015

The governing equation describing 3-D transient head distribution in a homogeneous and anisotropic aquifer is expressed as

$$K_x \frac{\partial^2 h}{\partial x^2} + K_y \frac{\partial^2 h}{\partial y^2} + K_z \frac{\partial^2 h}{\partial z^2} = S_s \frac{\partial h}{\partial t} \quad (1)$$

where t is time, $h(x, y, z, t)$ represents the hydraulic head, K_x, K_y, and K_z are the hydraulic conductivities in x, y, and z directions, respectively, and S_s is the specific storage. The initial static water table is chosen as the reference datum where the elevation head is set to zero. The initial condition is therefore written as

$$h = 0 \quad \text{at} \quad t = 0 \quad (2)$$

The Robin conditions specified at the four sides of the aquifer are defined as

$$\frac{\partial h}{\partial x} - \frac{K_1}{K_x b_1} h = 0 \quad \text{at} \quad x = 0 \quad (3)$$

$$\frac{\partial h}{\partial x} + \frac{K_2}{K_x b_2} h = 0 \quad \text{at} \quad x = l \quad (4)$$

$$\frac{\partial h}{\partial y} - \frac{K_3}{K_y b_3} h = 0 \quad \text{at} \quad y = 0 \quad (5)$$

$$\frac{\partial h}{\partial y} + \frac{K_4}{K_y b_4} h = 0 \quad \text{at} \quad y = w \quad (6)$$

where the subscripts 1, 2, 3, and 4 represent the boundaries at $x = 0$, $x = l$, $y = 0$, and $y = w$, respectively, and K and b are the hydraulic conductivity and width of the medium between the aquifer and boundary, respectively. Note that each of Eqs. (3)–(6) reduces to the Dirichlet condition when b (i.e., b_1, b_2, b_3 or b_4) is set to zero and the no-flow condition when K (i.e., K_1, K_2, K_3 or K_4) is set to zero. The aquifer lies on an impermeable base denoted as

$$\partial h / \partial z = 0 \quad \text{at} \quad z = -B. \quad (7)$$

HESSD
12, 12247–12280, 2015

The first-order free surface equation describing the response of water table to recharge over the rectangular region can be written as (Zlotnik and Ledder, 1993)

$$K_z \frac{\partial h}{\partial z} + S_y \frac{\partial h}{\partial t} = I u_x u_y \quad \text{at} \quad z = 0 \tag{8}$$

$$u_x = u(x - x_1) - u(x - x_1 - a) \tag{8a}$$

$$u_y = u(y - y_1) - u(y - y_1 - b) \tag{8b}$$

where S_y is the specific yield, I is a recharge rate, and u is the unit step function. Equation (8) involves the simplification from non-uniform saturated aquifer thickness below $z = h$ to uniform one below $z = 0$. Marino (1967) indicated that the simplification is valid when the water table rise is smaller than 50 % of the initial water table height and the recharge rate is smaller than 20 % of the hydraulic conductivity.

Dimensionless variables and parameters are defined as follows

$$\bar{h} = \frac{h}{B}, \bar{x} = \frac{x}{d}, \bar{y} = \frac{y}{d}, \bar{z} = \frac{z}{B}, \bar{I} = \frac{I}{d}, \bar{w} = \frac{w}{d}, \bar{x}_1 = \frac{x_1}{d}, \bar{y}_1 = \frac{y_1}{d}, \bar{a} = \frac{a}{d}, \bar{b} = \frac{b}{d}, \kappa_z = \frac{K_z d^2}{K_x B^2},$$
$$\bar{t} = \frac{K_x t}{S_s d^2}, \kappa_y = \frac{K_y}{K_x}, \kappa_1 = \frac{K_1 d}{K_x b_1}, \kappa_2 = \frac{K_2 d}{K_x b_2}, \kappa_3 = \frac{K_3 d}{K_y b_3}, \kappa_4 = \frac{K_4 d}{K_y b_4}, \xi = \frac{I}{K_z}, \varepsilon = \frac{S_y}{S_s B} \tag{9}$$

where the overbar denotes a dimensionless symbol. According to Eq. (9), the mathematical model, Eqs. (1)–(8b), can then be expressed as

$$\frac{\partial^2 \bar{h}}{\partial \bar{x}^2} + \kappa_y \frac{\partial^2 \bar{h}}{\partial \bar{y}^2} + \kappa_z \frac{\partial^2 \bar{h}}{\partial \bar{z}^2} = \frac{\partial \bar{h}}{\partial \bar{t}} \tag{10}$$

$$\bar{h} = 0 \quad \text{at} \quad \bar{t} = 0 \tag{11}$$

$$\frac{\partial \bar{h}}{\partial \bar{x}} - \kappa_1 \bar{h} = 0 \quad \text{at} \quad \bar{x} = 0 \tag{12}$$

HESSD
12, 12247–12280, 2015

$$\frac{\partial \overline{h}}{\partial \overline{x}} + \kappa_2 \overline{h} = 0 \quad \text{at} \quad \overline{x} = \overline{l} \tag{13}$$

$$\frac{\partial \overline{h}}{\partial \overline{y}} - \kappa_3 \overline{h} = 0 \quad \text{at} \quad \overline{y} = 0 \tag{14}$$

$$\frac{\partial \overline{h}}{\partial \overline{y}} + \kappa_4 \overline{h} = 0 \quad \text{at} \quad \overline{y} = \overline{w} \tag{15}$$

$$\partial \overline{h} / \partial \overline{z} = 0 \quad \text{at} \quad \overline{z} = -1 \tag{16}$$

$$\frac{\partial \overline{h}}{\partial \overline{z}} + \frac{\varepsilon}{\kappa_z} \frac{\partial \overline{h}}{\partial \overline{t}} = \xi \overline{u}_x \overline{u}_y \quad \text{at} \quad \overline{z} = 0 \tag{17}$$

$$\overline{u}_x = u\left(\overline{x} - \overline{x}_1\right) - u\left(\overline{x} - \overline{x}_1 - \overline{a}\right) \tag{17a}$$

$$\overline{u}_y = u\left(\overline{y} - \overline{y}_1\right) - u\left(\overline{y} - \overline{y}_1 - \overline{b}\right). \tag{17b}$$

2.2 Analytical solution

The solution of the model is derived by applying the Laplace transform and the double-integral transform to Eqs. (10)–(17b) and then inverting the transformed results with the complex integral and the inverse formulas of double-integral transform. The solution is expressed as

$$\overline{h}(\overline{x}, \overline{y}, \overline{z}, \overline{t}) = \sum_{m=1}^{\infty} \sum_{n=1}^{\infty} \Phi\left(\alpha_m, \beta_n, \overline{z}, \overline{t}\right) F_x\left(\alpha_m, \overline{x}\right) F_y\left(\beta_n, \overline{y}\right) \tag{18}$$

with

$$\Phi = \phi_s + \phi_0 + \sum_{j=1}^{\infty} \phi_j \tag{18a}$$

HESSD
12, 12247–12280, 2015

$$\phi_s = \frac{R_e \cosh\left[\left(1+\overline{z}\right)\lambda_s\right]}{\kappa_z \lambda_s \sinh(\lambda_s)} \tag{18b}$$

$$\phi_0 = -2\lambda_0 R_e \cosh\left[\left(1+\overline{z}\right)\lambda_0\right] \exp\left(-\gamma_0 \overline{t}\right)/\eta_0 \tag{18c}$$

$$\phi_j = -2\lambda_j R_e \cos\left[\left(1+\overline{z}\right)\lambda_j\right] \exp\left(-\gamma_j \overline{t}\right)/\eta_j \tag{18d}$$

$$\eta_0 = \gamma_0[(1+2\varepsilon\kappa_z)\lambda_0 \cosh(\lambda_0) + (1-\varepsilon\gamma_0)\sinh(\lambda_0)] \tag{18e}$$

$$\eta_j = \gamma_j[(1+2\varepsilon\kappa_z)\lambda_j \cos\left(\lambda_j\right) + \left(1-\varepsilon\gamma_j\right)\sin(\lambda_j)] \tag{18f}$$

$$\lambda_s = \sqrt{f/\kappa_z}, \gamma_0 = f - \kappa_z\lambda_0^2, \gamma_j = f + \kappa_z\lambda_j^2 \tag{18g}$$

$$R_e = \xi U_x(\alpha_m) U_y(\beta_n) \tag{18h}$$

$$U_x(\alpha_m) = \frac{\sqrt{2}V_x(\alpha_m)}{\sqrt{\kappa_1 + \left(\alpha_m^2 + \kappa_1^2\right)\left[\overline{l} + \kappa_2/\left(\alpha_m^2 + \kappa_2^2\right)\right]}} \tag{18i}$$

$$U_y(\beta_n) = \frac{\sqrt{2}V_y(\beta_n)}{\sqrt{\kappa_3 + \left(\beta_n^2 + \kappa_3^2\right)\left[\overline{w} + \kappa_4/\left(\beta_n^2 + \kappa_4^2\right)\right]}} \tag{18j}$$

$$V_x(\alpha_m) = \left\{\kappa_1\left[\cos\left(\alpha_m \overline{x}_1\right) - \cos\left(\alpha_m \chi\right)\right] - \alpha_m\left[\sin\left(\alpha_m \overline{x}_1\right) - \sin\left(\alpha_m \chi\right)\right]\right\}/\alpha_m \tag{18k}$$

$$V_y(\beta_n) = \left\{\kappa_3\left[\cos\left(\beta_n \overline{y}_1\right) - \cos\left(\beta_n \psi\right)\right] - \beta_n\left[\sin\left(\beta_n \overline{y}_1\right) - \sin\left(\beta_n \psi\right)\right]\right\}/\beta_n \tag{18l}$$

$$F_x\left(\alpha_m, \overline{x}\right) = \frac{\sqrt{2}\left[\alpha_m \cos\left(\alpha_m \overline{x}\right) + \kappa_1 \sin\left(\alpha_m \overline{x}\right)\right]}{\sqrt{\kappa_1 + \left(\alpha_m^2 + \kappa_1^2\right)\left[\overline{l} + \kappa_2/\left(\alpha_m^2 + \kappa_2^2\right)\right]}} \tag{18m}$$

$$F_y\left(\beta_n, \overline{y}\right) = \frac{\sqrt{2}\left[\beta_n \cos\left(\beta_n \overline{y}\right) + \kappa_3 \sin\left(\beta_n \overline{y}\right)\right]}{\sqrt{\kappa_3 + \left(\beta_n^2 + \kappa_3^2\right)\left[\overline{w} + \kappa_4/\left(\beta_n^2 + \kappa_4^2\right)\right]}} \tag{18n}$$

HESSD
12, 12247–12280, 2015

$$f = \alpha_m^2 + \kappa_y \beta_n^2, \chi = \overline{x}_1 + \overline{a}, \psi = \overline{y}_1 + \overline{b} \tag{18o}$$

where subscripts m, n, and j are integers varying from 1, 2, ... ∞, and eigenvalues α_m, β_n, λ_j, and λ_0 are the positive roots of the following equations, respectively, as

$$\tan\left(\overline{l}\alpha_m\right) = \frac{\alpha_m(\kappa_1 + \kappa_2)}{\alpha_m^2 - \kappa_1\kappa_2} \tag{19}$$

$$\tan\left(\overline{w}\beta_n\right) = \frac{\beta_n(\kappa_3 + \kappa_4)}{\beta_n^2 - \kappa_3\kappa_4} \tag{20}$$

$$\tan(\lambda_j) = -\varepsilon\left(f + \kappa_z\lambda_j^2\right)/\lambda_j \tag{21}$$

$$\frac{-\varepsilon\kappa_z\lambda_0^2 + \lambda_0 + \varepsilon f}{\varepsilon\kappa_z\lambda_0^2 + \lambda_0 - \varepsilon f} = \exp(2\lambda_0) \tag{22}$$

The detailed development of Eq. (18) is demonstrated in Appendix. Additionally, Eqs. (19)–(21) have infinite roots owing to the trigonometric function tan whereas Eq. (22) has only one positive root. The schemes to search for the roots α_m, β_n, λ_j, and λ_0 are introduced in the following section. The first and second terms on the right-hand side (RHS) of Eq. (18) are double series expanded by α_m and β_n. The RHS third term in Eq. (18) is triple series expanded by α_m, β_n, and λ_j.

The use of finite aquifer domain has two merits. One is that the solution of depth-average head, defined as $\int_{-1}^{0}\overline{h}(\overline{x},\overline{y},\overline{z},\overline{t})\mathrm{d}\overline{z}$, can be analytically integrated. The integration variable $\overline{z}$ appears only in the functions of $\cosh\left[(1+\overline{z})\lambda_s\right]$ in Eq. (18b), $\cosh\left[(1+\overline{z})\lambda_0\right]$ in Eq. (18c) and $\cos\left[(1+\overline{z})\lambda_j\right]$ in Eq. (18d). The solution of depth-average head therefore equals Eq. (18) where these three functions are replaced by $\sinh(\lambda_s)/\lambda_s$, $\sinh(\lambda_0)/\lambda_0$, and $\sin(\lambda_j)/\lambda_j$, respectively. The other is that the present solution is applicable to head predictions in aquifers of infinite extent before the dimensionless time to have lateral aquifer boundary effect on the head distribution. Wang and

HESSD
12, 12247–12280, 2015

Yeh (2008) mentioned a time criterion defined as $\overline{t}_{cr} = 0.03(1+\varepsilon)\overline{R}^2$ where $\overline{R} = R/d$ denotes a shortest dimensionless distance from the lateral boundary to the edge of the recharge region. This criterion is, in effect, a boundary-effect time representing a time that the head distribution starts to have the effect of the aquifer boundary. Existing solutions based on aquifers of infinite extent can therefore be considered as special cases of the present solution if the dimensionless recharge time is less than the boundary-effect time.

2.3 Calculation of eigenvalues

The eigenvalues α_m, β_n, λ_j, and λ_0 can be determined by Newton's method with initial guess values (IGVs) set to be the vertical asymptotes of the functions on the left-hand side (LHS) of Eqs. (19)–(22), respectively. Hence, IGVs for α_m are $\alpha' + \delta$ if $\alpha' < (\kappa_1\kappa_2)^{1/2}$ and $\alpha' - \delta$ if $\alpha' > (\kappa_1\kappa_2)^{1/2}$ where $\alpha' = (2m-1)\pi/(2\overline{l})$ and δ is a small value of 10^{-8} to avoid being right at the vertical asymptotes. Similarly, IGVs for β_n are $\beta' + \delta$ if $\beta' < (\kappa_3\kappa_4)^{1/2}$ and $\beta' - \delta$ if $\beta' > (\kappa_3\kappa_4)^{1/2}$ where $\beta' = (2n-1)\pi/(2\overline{w})$. In addition, IGVs for λ_j are $(2j-1)\pi/2 + \delta$, and IGV for λ_0 is $\delta + \left[\left(1 + 4\kappa_z f \varepsilon^2\right)^{1/2} - 1\right]/(2\varepsilon\kappa_z)$ obtained by setting the denominator of the LHS function of Eq. (22) to be zero.

2.4 Solution for time-varying recharge rate

The present solution, Eq. (18), is applicable to arbitrary time-depending recharge rates on the basis of the convolution technique expressed as

$$\overline{h}_{It} = \overline{h}_{I0} + \int_0^{\overline{t}} \frac{\partial \xi_t(\tau)}{\partial \tau} \overline{h}\left(\overline{t} - \tau\right)/\xi \, \mathrm{d}\tau \tag{23}$$

HESSD
12, 12247–12280, 2015

where $\overline{h}_{It}$ signifies a dimensionless head solution for a time-depending recharge rate, $\xi_t(\tau)$ represents a dimensionless transient recharge rate, τ is a dummy variable, $\overline{h}_{I0}$ is Eq. (18) in which ξ in Eq. (18h) is replaced by $\xi_t(0)$, and $\overline{h}(\bar{t}-\tau)$ is also Eq. (18) with $\bar{t}$ replaced by $\bar{t}-\tau$. If Eq. (23) is not integrable, it can be discretized as (Singh, 2005)

$$\overline{h}_{\mathrm{N}} = \sum_{i=1}^{N} \frac{\Delta\xi_i}{\Delta\bar{t}} \eta(N-i+1) \tag{24}$$

with

$$\Delta\xi_i = \xi_i - \xi_{i-1} \tag{24a}$$

$$\eta(M) = \int_0^{\bar{t}} \overline{h}(M\Delta\bar{t}-\tau)\mathrm{d}\tau \tag{24b}$$

where $\overline{h}_{\mathrm{N}}$ represents a numerical result of dimensionless head $\overline{h}$ at $\bar{t} = \Delta\bar{t} \times N$, $\Delta\bar{t}$ is a dimensionless time step, ξ_i and ξ_{i-1} are dimensionless recharge rates at $\bar{t} = \Delta\bar{t} \times i$ and $\bar{t} = \Delta\bar{t} \times (i-1)$, respectively, and $\eta(M)$, called ramp kernel, depends on Eq. (18) in which $\bar{t}$ is replaced by $M\Delta\bar{t}-\tau$. The integration result of Eq. (24b) can be denoted as Eq. (18) where ϕ_s is replaced by $\phi_s\bar{t}$ and two exponential terms in Eqs. (18c) and (18d) are replaced, respectively, by $\exp\left(-M\gamma_0\Delta\bar{t}\right)\left[-1+\exp\left(\gamma_0\Delta\bar{t}\right)\right]/\gamma_0$ and $\exp\left(-M\gamma_j\Delta\bar{t}\right)\left[-1+\exp\left(\gamma_j\Delta\bar{t}\right)\right]/\gamma_j$.

2.5 Sensitivity analysis

The sensitivity analysis is administered to assess the change in the hydraulic head in response to the change in each of the hydraulic parameters. A coefficient to denote the

HESSD
12, 12247–12280, 2015

sensitivity of the hydraulic head to a specific parameter can be expressed as

$$S_{c,t} = \frac{\partial h/B}{\partial P_c/P_c} = P_c \frac{\partial \overline{h}}{\partial P_c} \tag{25}$$

where P_c is the cth parameter in the present solution, $S_{c,t}$ is the normalized sensitivity coefficient at a time to the $c-$ th parameter, and $\overline{h}$ is the present solution, Eq. (18). The derivative in Eq. (25) can be approximated as

$$S_{c,t} = \frac{\overline{h}(P_c + \Delta P_c) - \overline{h}(P_c)}{\Delta P_c/P_c} \tag{26}$$

where ΔP_c is an increment chosen as $10^{-3}\Delta P_c$ (Yeh et al., 2008).

3 Results and discussion

Previous articles have discussed groundwater mounds in response to localized recharge into aquifers with various hydraulic parameters (e.g., Dagan, 1967; Rao and Sarma, 1980; Latinopoulos, 1986; Manglik et al., 1997; Manglik and Rai, 1998; Rai et al., 1998; Chang and Yeh, 2007; Illas et al., 2008; Bansal and Das, 2010; Bansal and Teloglou, 2013). Flow velocity fields below groundwater mounds have also been analyzed (Zlotnik and Ledder, 1992, 1993). This section therefore focuses on the transient behavior of hydraulic head at an observation well with the aid of the present solution. The default values of the parameters and variables for calculation are noted in Table 2. In Sect. 3.1, transient head distributions in aquifers subject to Dirichlet, no-flow and Robin boundary conditions are compared. In Sect. 3.2, the effect of the vertical flow on the head distribution is investigated. In Sect. 3.3, errors arising from assuming aquifer incompressibility (i.e., $S_s = 0$) to develop analytical solutions is discussed. In Sect. 3.4, the response of the hydraulic head to transient recharge rates based on Eq. (23) is demonstrated. In Sect. 3.5, the sensitivity analysis defined by Eq. (26) is performed.

HESSD
12, 12247–12280, 2015

3.1 Effect of lateral boundary

The Robin condition can become the Dirichlet or no-flow one, depending on the magnitudes of $\kappa_1\overline{d}_1$ for Eq. (12), $\kappa_2\overline{d}_2$ for Eq. (13), $\kappa_3\overline{d}_3$ for Eq. (14), and $\kappa_4\overline{d}_4$ for Eq. (15). We consider a symmetrical aquifer system with $\overline{l} = \overline{w} = 22$, $\overline{d}_1 = \overline{d}_2 = \overline{d}_3 = \overline{d}_4 = 10$ and $\kappa_1 = \kappa_2 = \kappa_3 = \kappa_4$ as illustrated in Fig. 2. The magnitudes of $\kappa_1\overline{d}_1$, $\kappa_2\overline{d}_2$, $\kappa_3\overline{d}_3$ and $\kappa_4\overline{d}_4$ are the same and defined as κ. The curves of $\overline{h}$ vs. $\overline{t}$ plotted by the present solution, Eq. (18), for $\kappa = 10^{-3}$, 10^{-2}, 10^{-1}, 1, 10, 100, and 200 are shown in Fig. 2. The curves $\overline{h}$ vs. $\overline{t}$ are plotted from Manglik et al. (1997) solution with the no-flow condition (i.e., $\kappa = 0$), Manglik and Rai (1998) solution with the Dirichlet condition (i.e., $\kappa \to \infty$), and the present solution with the Robin condition. Before $\overline{t} = 10^4$, these curves give the same magnitude of $\overline{h}$ at a fixed dimensionless time $\overline{t}$ since the lateral aquifer boundary has been beyond where groundwater is affected by localized recharge. After $\overline{t} = 10^4$, the curves for the cases of $\kappa = 10^{-2}$, 10^{-1}, 1, 10, and 100 deviate from each other gradually as time increases. A larger magnitude of κ between $\kappa = 10^{-2}$ and $\kappa = 100$ causes a smaller $\overline{h}$ at a fixed $\overline{t}$. On the other hand, the present solution for the cases of $\kappa = 10^{-3}$ and 10^{-2} agrees well with Manglik et al. (1997) solution based on $\kappa = 0$ and for the cases of $\kappa = 100$ and 200 predicts the same result as Manglik and Rai (1998) solution based on $\kappa \to \infty$. We may reasonably conclude that the Robin condition reduces to the no-flow one when $\kappa \leq 10^{-2}$ and the Dirichlet one when $\kappa \geq 100$.

3.2 Effect of vertical flow

Dimensionless parameter κ_z (i.e., $K_z d^2 / \left(K_x B^2\right)$) dominates the effect of the vertical flow on transient head distributions at an observation well. Consider $\kappa_1\overline{d}_1 = \kappa_2\overline{d}_2 = \kappa_3\overline{d}_3 = \kappa_4\overline{d}_4 = 100$ for lateral aquifer boundaries under the Dirichlet condition as discussed in Sect. 3.1. The temporal distributions of $\overline{h}$ predicted by the present solution, Eq. (18), with $\kappa_z = 0.01$, 0.1, 1, and 10 are demonstrated in Fig. 3. The temporal dis-

HESSD
12, 12247–12280, 2015

tribution of $\overline{h}$ predicted by Manglik and Rai (1998) solution based on 2-D flow without the vertical component is taken in order to address the effect of vertical flow. The figure reveals that $\overline{h}$ increases with κ_z when $\kappa_z \leq 1$. The difference in $\overline{h}$ predicted by both solutions indicates the vertical flow effect. The Manglik and Rai (1998) solution obviously overestimates the head. The vertical flow prevails, and its effect should be taken into account when $\kappa_z < 1$, indicating a thick aquifer, a small ratio of K_z/K_x, and/or an observation well near a recharge region. On the other hand, the present solution for the cases of $\kappa_z = 1$ and 10 agrees well with Manglik and Rai (1998) solution, indicating that the vertical flow effect is ignorable when $\kappa_z \geq 1$. We can recognize from the agreement that existing solutions neglecting the vertical flow effect give good predictions when $\kappa_z \geq 1$.

3.3 Effect of specific storage

Some of existing models use the Laplace equation as a governing equation with assuming $S_s = 0$ (e.g., Singh, 1976; Schmitz and Edenhofer, 1988; Zlotnik and Ledder, 1993). The assumption is valid when ε (i.e., $S_y/(S_s B)$) is larger than a certain value. This section quantifies the value. The Zlotnik and Ledder (1993) model based on 3-D Laplace equation, Eq. (1) with $S_s = 0$, is taken for comparison with the present model using Eq. (1) with $S_s \neq 0$. The dimensionless variables of s, x, y, z, t, X, and Y in their model are replaced by $\overline{h}/\xi$, $(\kappa_z)^{1/2}\overline{x}$, $(\kappa_z)^{1/2}\overline{y}$, $\overline{z}$, $\kappa_z\overline{t}/\varepsilon$, $(\kappa_z)^{1/2}\overline{a}$, and $(\kappa_z)^{1/2}\overline{b}$, respectively, for ease of comparisons. Consider the cases of $\kappa_z = 10^{-2}$ for an observation well located at a 3-D flow area and $\kappa_z = 10$ for the well located at a 2-D flow area as discussed in Sect. 3.2. The assumption can be assessed through the comparison in the dimensionless heads predicted by both solutions for $\varepsilon = 1$, 10, 10^2, and 10^3 as shown in Fig. 4a for $\kappa_z = 10^{-2}$ and Fig. 4b for $\kappa_z = 10$. The present solution predicts a steady-state $\overline{h}$ of 0.054 in Fig. 4a and 0.074 in Fig. 4b after certain times due to lateral Dirichlet boundaries (i.e., $\kappa_1\overline{d}_1 = \kappa_2\overline{d}_2 = \kappa_3\overline{d}_3 = \kappa_4\overline{d}_4 = 100$) as discussed in Sect. 3.1. In contrast, their solution predicts $\overline{h}$ which increases with $\overline{t}$ due to the absence of lat-

HESSD
12, 12247–12280, 2015

eral boundaries. When $\varepsilon = 1$ and 10, both solutions give different values of $\overline{h}$ for both cases of $\kappa_z = 10^{-2}$ and $\kappa_z = 10$ before $\overline{t} = 100$, indicating that the assumption of $S_s = 0$ causes inaccurate $\overline{h}$. When $\varepsilon = 10^2$ and 10^3, both solutions predict very close results of $\overline{h}$ for both cases before the time of approaching steady-state $\overline{h}$. These results lead to the conclusion that the assumption of $S_s = 0$ is valid when $\varepsilon \geq 100$ for 3-D and 2-D flow cases.

3.4 Transient recharge rate

Most articles (e.g., Rai et al., 1998; Chang and Yeh, 2007; Illas et al., 2008; Bansal and Teloglou, 2013) define a transient recharge rate as $I_t(t) = I_1 + I_0 \exp(-rt)$ (i.e., $\xi_t(\overline{t}) = \xi_1 + \xi_0 \exp(-\gamma \overline{t})$ for a dimensionless rate) where $\xi_t = I_t/K_z$, $\xi_1 = I_1/K_z$, $\xi_0 = I_0/K_z$, $\gamma = rS_s d^2/K_x$, and r is a decay constant. The rate decays exponentially from an initial value of $I_1 + I_0$ to an ultimate one of I_1. The present solution, Eq. (18), can be applied for the response of the head to the transient rate based on Eq. (23). Substituting $\partial \xi_t(\tau)/\partial \tau = -\gamma \xi_0 \exp(-\gamma \tau)$ into Eq. (23) and integrating the result for τ from $\tau = 0$ to $\tau = \overline{t}$ yields the present solution of the dimensionless head accounting for the transient rate, giving $\overline{h}_{I0}$ plus Eq. (18) where R_e in Eqs. (18b), $R_e \exp(-\gamma_0 \overline{t})$ in Eq. (18c), and $R_e \exp(-\gamma_j \overline{t})$ in Eq. (18d) are replaced by $R_0[\exp(-\gamma \overline{t}) - 1]$, $\gamma R_0 \left[\exp(-\gamma \overline{t}) - \exp\left(\gamma_0 \overline{t}\right)\right]/(\gamma_0 + \gamma)$, and $\gamma R_0 \left[\exp(-\gamma \overline{t}) - \exp\left(\gamma_j \overline{t}\right)\right]/(\gamma_j + \gamma)$ with $R_0 = \xi_0 U_x(\alpha_m) U_y(\beta_n)$, respectively. Similarly, Zlotnik and Ledder (1993) solution can also be used to obtain the head subject to the transient rate by substituting it into Eq. (23) and then integrating the result using numerical approaches. Now, we consider Ramana et al. (1995) solution depicting 2-D flow induced by the transient rate in rectangular aquifers with the lateral boundary under the Dirichlet condition. Figure 5 shows the temporal distributions of $\overline{h}$ for the transient rate predicted by these three solutions when $\kappa_z = 1$, $\kappa = 100$ and $\varepsilon = 100$. The present solution agrees well with Ramana et al. (1995) solution. We can recognize

HESSD
12, 12247–12280, 2015

from the agreement that, even for transient rates, the Robin condition reduces to the Dirichlet one when $\kappa \geq 100$ (i.e., $\kappa_1\overline{d}_1 = \kappa_2\overline{d}_2 = \kappa_3\overline{d}_3 = \kappa_4\overline{d}_4 = 100$) as discussed in Sect. 3.1 and the vertical flow effect is ignorable when $\kappa_z \geq 1$ as discussed in Sect. 3.2. Moreover, agreement on $\overline{h}$ estimated by the present solution and Zlotnik and Ledder (1993) solution before $\overline{t} = 3\times10^3$ will make clear that, even for transient rates, assuming aquifer incompressibility (i.e., $S_s = 0$) is valid when $\varepsilon \geq 100$ as discussed in Sect. 3.3.

3.5 Sensitivity analysis

Consider point A of (555, 500, −10 m) at a 3-D flow region (i.e., $\kappa_z < 1$) and point B of (800, 500, −10 m) at a 2-D flow region (i.e., $\kappa_z \geq 1$) as discussed in Sect. 3.2. Localized recharge distributes over the squire area of 450 m $\leq x \leq$ 550 m and 450 m $\leq y \leq$ 550 m. The distance d herein is set to 5 m for point A and 250 m for point B. The aquifer system is of isotropy with $K_x = K_y$ and symmetry with $K_1 = K_2 = K_3 = K_4$ for conciseness. The sensitivity analysis is performed by Eq. (26) to investigate the responses of the hydraulic heads at these two points to the change in each of a, b, S_s, S_y, K_x (or K_y), K_z, and K_1 (or K_2, K_3 and K_4). The curves of the normalized sensitivity coefficient $S_{c,t}$ vs. t for these seven parameters are shown in Fig. 6a for point A and Fig. 6b for point B. The figure shows that the hydraulic heads at both points are more sensitive to the changes in a, b, K_x, and S_y than those in the others. This may indicate that a flow model should include at least these four parameters. The figure also shows that the heads at points A and B are insensitive to the change in K_1 because of $\kappa_1\overline{d}_1 = 4500 > 100$ as discussed in Sect. 3.1. In addition, $S_{c,t}$ to K_z for point A is nonzero after $t = 0.4$ day due to $\kappa_z = 6.25\times10^{-3} < 1$ as discussed in Sect. 3.2. In contrast, $S_{c,t}$ to K_z for point B is very close to zero over the entire period because of $\kappa_z = 15.625 > 1$. Moreover, the heads at points A and B are insensitive to the change in S_s due to $\varepsilon = 500 > 100$ as discussed in Sect. 3.3.

HESSD
12, 12247–12280, 2015

4 Concluding remarks

A mathematical model is developed to depict spatiotemporal head distributions induced by localized recharge with an arbitrary time-varying rate in a rectangular unconfined aquifer bounded by Robin boundaries with different hydraulic parameters. A governing equation for 3-D flow is considered. A first-order free surface equation with a source term representing the recharge is employed for describing the change in water table. The analytical head solution of the model is obtained by applying the Laplace transform, the double-integral transform, and the convolution technique. The use of rectangular aquifer domain leads to two merits. One is that the integration for the solution of the depth-average head can be analytically done. The other is that existing solutions based on aquifers of infinite extent are special cases of the present solution when the recharge time is less than the boundary-effect time. The sensitivity analysis is performed to explore the response of the head to the change in each of hydraulic parameters. With the aid of the present solution, the following conclusions can be drawn:

1. In respect of affecting $\overline{h}$ at observation wells, the Robin condition specified at $\overline{x} = 0$ reduces to the Dirichlet one when $\kappa_1 \overline{d}_1 \geq 100$ (i.e., $K_1 d_1/(K_x b_1) \geq 100$) and no-flow one when $\kappa_1 \overline{d}_1 \leq 10^{-2}$. The quantitative criteria for $\kappa_1 \overline{d}_1$ are applicable to $\kappa_2 \overline{d}_2$, $\kappa_3 \overline{d}_3$, and $\kappa_4 \overline{d}_4$ for the Robin conditions specified at $\overline{x} = \overline{l}$, $\overline{y} = 0$, and $\overline{y} = \overline{w}$, respectively.

2. The vertical flow causes significant decrease in the hydraulic head at an observation well when $\kappa_z < 1$ (i.e., $K_z d^2 / \left(K_x B^2\right) < 1$). When $\kappa_z \geq 1$, the effect of vertical flow on the head is ignorable, and conventional models considering 2-D flow without the vertical component can therefore predict accurate results.

3. The 3-D Laplace equation based on the assumption of $S_s = 0$ can be regarded as a flow governing equation when $\varepsilon \geq 100$ (i.e., $S_y/(S_s B) \geq 100$) for the whole

HESSD
12, 12247–12280, 2015

aquifer domain. Otherwise, the hydraulic head based on the Laplace equation is overestimated.

4. The abovementioned conclusions are also applicable to problems of groundwater flow subject to recharge with arbitrary time-varying rates.

Appendix: Derivation of Eq. (18)

The applications of the Laplace transform to $\overline{h}$ and $\partial\overline{h}/\partial\overline{t}$ lead, respectively, to

$$\widetilde{h} = \int_0^\infty \overline{h}\exp(-p\overline{t})\mathrm{d}\overline{t} \tag{A1}$$

and

$$\int_0^\infty \frac{\partial\overline{h}}{\partial\overline{t}}\exp(-p\overline{t})\mathrm{d}\overline{t} = p\widetilde{h} - \overline{h}|_{\overline{t}=0} \tag{A2}$$

where $\widetilde{h}$ represents the dimensionless head in the Laplace domain, p is the Laplace transform parameter, and $\overline{h}|_{\overline{t}=0}$ equals zero due to Eq. (11). The double-integral transform for the Robin conditions, Eqs. (12)–(15), is defined as (Latinopoulos, 1985; Table I, aquifer type 1)

$$\hat{h} = \int_0^{\overline{w}}\int_0^{\overline{l}} \widetilde{h}F_x\left(\alpha_m,\overline{x}\right)F_y\left(\beta_n,\overline{y}\right)\mathrm{d}\overline{x}\mathrm{d}\overline{y} \tag{A3}$$

where $F_x(\alpha_m,\overline{x})$ and $F_y(\beta_n,\overline{y})$, the kernel functions of the transform, are defined by Eqs. (18m) and (18n), respectively, α_m and β_n are the roots of Eqs. (19) and (20),

HESSD
12, 12247–12280, 2015

respectively. The double-integral transform has property

$$\int_0^{\overline{w}}\int_0^{\overline{l}}\left(\frac{\partial^2\widetilde{h}}{\partial\overline{x}^2}+\kappa_y\frac{\partial^2\widetilde{h}}{\partial\overline{y}^2}\right)F_x\left(\alpha_m,\overline{x}\right)F_y\left(\beta_n,\overline{y}\right)\mathrm{d}\overline{x}\mathrm{d}\overline{y}=-\left(\alpha_m^2+\kappa_y\beta_n^2\right)\hat{h} \tag{A4}$$

where $\partial^2\widetilde{h}/\partial\overline{x}^2+\kappa_y\left(\partial^2\widetilde{h}/\partial\overline{y}^2\right)$ is obtained by applying the Laplace transform to Eq. (10). Note that Eq. (A4) is based on Eqs. (12)–(15) with constants equaling zero.

The model, Eqs. (10)–(17b), after taking the Laplace transform can be written as Eqs. (10) and (12)–(17b) where $\overline{h}$ and $\partial\overline{h}/\partial\overline{t}$ are replaced by $\widetilde{h}$ and $p\widetilde{h}$, respectively, according to Eqs. (A1) and (A2). The application of the double-integral transform (i.e., Eqs. A3 and A4) to the resultant model then yields

$$\kappa_z\frac{\partial^2\hat{h}}{\partial\overline{z}^2}-\left(p+\alpha_m^2+\kappa_y\beta_n^2\right)\hat{h}=0 \tag{A5}$$

$$\partial\hat{h}/\partial\overline{z}=0 \quad \text{at} \quad \overline{z}=-1 \tag{A6}$$

$$\frac{\partial\hat{h}}{\partial\overline{z}}+\frac{\varepsilon p}{\kappa_z}\hat{h}=\frac{\xi}{p}U_x\left(\alpha_m\right)U_y\left(\beta_n\right) \quad \text{at} \quad \overline{z}=0 \tag{A7}$$

where $U_x\left(\alpha_m\right)$ and $U_y\left(\beta_n\right)$ are defined in Eqs. (18i) and (18j), respectively. Solving Eq. (A5) with Eqs. (A6) and (A7) results in the semi-analytical solution of $\hat{h}$ denoted as

$$\hat{h}\left(\alpha_m,\beta_n,\overline{z},p\right)=\frac{R_e\cosh[(1+\overline{z})\lambda]}{p\sigma(p)} \quad \text{for} \quad -1\le\overline{z}\le 0 \tag{A8}$$

with

$$\lambda=\sqrt{(p+f)/\kappa_z} \tag{A9}$$

$$\sigma(p)=p\varepsilon\kappa_z\cosh(\lambda)+\kappa_z\lambda\sinh(\lambda) \tag{A10}$$

HESSD
12, 12247–12280, 2015

where R_e and f are defined in Eqs. (18h) and (18o), respectively.

The time-domain solution, Eq. (18), is derived by applying the inverse Laplace and double-integral transforms to Eq. (A8). The former inversion of Eq. (A8) is first addressed below. Equation (A8) is a single-value function to p in a complex plane because satisfying $\hat{h}(p^+) = \hat{h}(p^-)$ where p^+ and p^- are in terms of the polar coordinates defined, respectively, as

$$p^+ = r_a \exp(i\theta) - f \tag{A11}$$

and

$$p^- = r_a \exp[i(\theta - 2\pi)] - f \tag{A12}$$

in which r_a represents a radius from the origin at $p = -f$, i herein is the imaginary unit, and θ is an argument between 0 and 2π. Substitutions of Eqs. (A11) and (A12) into Eq. (A9) lead, respectively, to

$$\lambda = \sqrt{r_a/\kappa_z}\exp(i\theta/2) = \sqrt{r_a/\kappa_z}[\cos(\theta/2) + i\sin(\theta/2)] \tag{A13}$$

and

$$\lambda = \sqrt{r_a/\kappa_z}\exp[i(\theta - 2\pi)/2] = -\sqrt{r_a/\kappa_z}[\cos(\theta/2) + i\sin(\theta/2)]. \tag{A14}$$

Substitution of Eqs. (A11) and (A13) or Eqs. (A12) and (A14) into Eq. (A8) gives rise to the same result. Equation (A8) is therefore a single-value function without branch cut, and its inverse Laplace transform equals the sum of residues for poles in the complex plane.

The residue for a simple pole can be formulated as

$$\text{Res} = \lim_{p\to\varphi} \hat{h}(p) \times (p - \varphi) \tag{A15}$$

HESSD
12, 12247–12280, 2015

where φ is the location of the pole in the complex plane, and $\hat{h}(p)$ is defined in Eq. (A8). The locations of infinite simple poles can be defined as the roots of the equation

$$p[p\varepsilon\kappa_z \cosh(\lambda) + \kappa_z \lambda \sinh(\lambda)] = 0 \tag{A16}$$

which is obtained by letting the denominator of the RHS in Eq. (A8) to be zero. Obviously, one pole is at $p = 0$ (i.e., $\varphi = 0$), and its residue equals the RHS in Eq. (18b) on the basis of Eq. (A15). Other poles exist at the negative part of the real axis in the complex plane, and their locations can be defined as the roots of the following equation

$$p\varepsilon\kappa_z \cosh(\lambda) + \kappa_z \lambda \sinh(\lambda) = 0 \tag{A17}$$

which is derived from Eq. (A16). One pole is at $p = \gamma_0$ (i.e., $\varphi = \gamma_0$) between $p = 0$ and $p = -f$. Substituting $p = \gamma_0$ and $\lambda = \lambda_0$ into Eq. (A9) results in $\lambda_0 = \sqrt{(\gamma_0 + f)/\kappa_z}$, which indicates the pole located at $\gamma_0 = -f + \kappa_z \lambda_0^2$. Equation (22) can be derived by the substitution of $\lambda = \lambda_0$ and $p = -f + \kappa_z \lambda_0^2$ (due to $p = \gamma_0$) into Eq. (A17) and the relationships of $\cosh(\lambda_0) = [\exp(\lambda_0) + \exp(-\lambda_0)]/2$ and $\sinh(\lambda_0) = [\exp(\lambda_0) - \exp(-\lambda_0)]/2$. The residue for the pole at $p = \gamma_0$ is defined as ϕ_0 in Eq. (18c) on the basis of Eq. (A15). On the other hand, infinite poles behind $p = -f$ are at $p = \gamma_j$ (i.e., $\varphi = \gamma_j$) where $j \in 1, 2, \ldots \infty$. Substituting $p = \gamma_j$ and $\lambda = i\lambda_j$ into Eq. (A9) obtains $\lambda_j i = \sqrt{(\gamma_j + f)/\kappa_z}$. This indicates those poles located at $\gamma_j = -f - \kappa_z \lambda_j^2$. Equation Eq. (21) can be derived by the substitution of $\lambda = i\lambda_j$ and $p = -f - \kappa_z \lambda_j^2$ (due to $p = \gamma_j$) into Eq. (A17) and the relationships of $\cosh(i\lambda_j) = cos(\lambda_j)$ and $\sinh(i\lambda_j) = i\sin(\lambda_j)$. The residue for the pole at $p = \gamma_j$ can be expressed as ϕ_j in Eq. (18d) in light of Eq. (A15). As a result, the inverse Laplace transform to Eq. (A8) is the sum of those residues, defined as $\Phi = \phi_s + \phi_0 + \sum_{j=1}^{\infty} \phi_j$. The inverse double-integral transform to Φ can be conducted by applying the formula of Eq. (18) (Latinopoulos, 1985; Eq. 14).

HESSD
12, 12247–12280, 2015

Acknowledgements. This study has been partly supported by the Taiwan Ministry of Science and Technology under the grants NSC 102-2221-E-009-072-MY2, MOST 103-2221-E-009-156, and NSC 104-2221-E-009 -148 -MY2.

References

Bansal, R. K. and Das, S. K.: Analytical study of water table fluctuation in unconfined aquifers due to varying bed slopes and spatial location of the recharge basin, J. Hydrol. Eng., 15, 909–917, 2010.

Bansal, R. K. and Teloglou, I. S.: An analytical study of groundwater fluctuations in unconfined leaky aquifers induced by multiple localized recharge and withdrawal, Global Nest. J., 15, 394–407, 2013.

Chang, Y. C. and Yeh, H. D.: Analytical solution for groundwater flow in an anisotropic sloping aquifer with arbitrarily located multiwells, J. Hydrol., 347, 143–152, 2007.

Chor, T. L. and Dias, N. L.: Technical note: a simple generalization of the Brutsaert and Nieber analysis, Hydrol. Earth Syst. Sc., 19, 2755–2761, 2015.

Dagan, G.: Linearized solutions of free surface groundwater flow with uniform recharge, J. Geophys. Res., 72, 1183–1193, 1967.

Hansen, B. P. and Lapham, W. W.: Geohydrology and simulated ground-water flow, Plymouth-Carver Aquifer, southeastern Massachusetts, Report, US Geological Survey, USA, 90–4204, 1992.

Hantush, M. S.: Growth of a ground water ridge in response to deep percolation, Symposium on Transient Ground water Hydraulics, Ft. Collins, Colorado, 25–27 July, 1963.

Hantush, M. S.: Growth and decay of groundwater-mounds in response to uniform percolation, Water Resour. Res., 3, 227–234, doi:10.1029/WR003i001p00227, 1967.

Hsieh, P. C., Hsu, H. T., Liao, C. B., and Chiueh, P. T.: Groundwater response to tidal fluctuation and rainfall in a coastal aquifer, J. Hydrol., 521, 132–140, 2015.

Illas, T. S., Thomas, Z. S., and Andreas, P. C.: Water table fluctuation in aquifers overlying a semi-impervious layer due to transient recharge from a circular basin, J. Hydrol., 348, 215–223, 2008.

Ireson, A. M. and Butler, A. P.: A critical assessment of simple recharge models: application to the UK Chalk, Hydrol. Earth Syst. Sc., 17, 2083–2096, 2013.

HESSD

12, 12247–12280, 2015

Latinopoulos, P.: Analytical solutions for periodic well recharge in rectangular aquifers with 3rd-kind boundary-conditions, J. Hydrol., 77, 293–306, 1985.
Latinopoulos, P.: Analytical solutions for strip basin recharge to aquifers with cauchy boundary-conditions, J. Hydrol., 83, 197–206, 1986.
Liang, X. Y. and Zhang, Y. K.: Analyses of uncertainties and scaling of groundwater level fluctuations, Hydrol. Earth Syst. Sc., 19, 2971–2979, 2015.
Liang, X. Y., Zhang, Y. K., and Schilling, K. E.: Analytical solutions for two-dimensional groundwater flow with subsurface drainage tiles, J. Hydrol., 521, 556–564, 2015.
Manglik, A. and Rai, S. N.: Two-dimensional modelling of water table fluctuations due to time-varying recharge from rectangular basin, Water Resour. Manag., 12, 467–475, 1998.
Manglik, A., Rai, S. N., and Singh, R. N.: Response of an Unconfined Aquifer Induced by Time Varying Recharge from a Rectangular Basin, Water. Resour. Manag., 11, 185–196, 1997.
Marino, M. A.: Hele-Shaw model study of the growth and decay of groundwater ridges, J. Geophys. Res., 72, 1195–1205, doi:10.1029/JZ072i004p01195, 1967.
Ostendorf, D. W., DeGroot, D. J., and Hinlein, E. S.: Unconfined aquifer response to infiltration basins and shallow pump tests, J. Hydrol., 338, 132–144, 2007.
Rai, S. N., Ramana, D. V., and Singh, R. N.: On the prediction of ground-water mound formation in response to transient recharge from a circular basin, Water Resour. Manag., 12, 271–284, 1998.
Rai, S. N., Manglik, A., and Singh, V. S.: Water table fluctuation owing to time-varying recharge, pumping and leakage, J. Hydrol., 324, 350–358, 2006.
Ramana, D. V., Rai, S. N., and Singh, R. N.: Water table fluctuation due to transient recharge in a 2-D aquifer system with inclined base, Water Resour. Manag., 9, 127–138, doi:10.1007/BF00872464, 1995.
Rao, N. H. and Sarma, P. B. S.: Growth of groundwater mound in response to Recharge, Ground Water, 18, 587–595, 1980.
Rao, N. H. and Sarma, P. B. S.: Recharge to aquifers with mixed boundaries, J. Hydrol., 74, 43–51, 1984.
Schmitz, G. and Edenhofer, J.: Semi analytical solution for the groundwater mound problem, Adv. Water Resour., 11, 21–24, 1988.
Singh, R.: Prediction of mound geometry under recharge basins, Water Resour. Res., 12, 775–780, doi:10.1029/WR012i004p00775, 1976.

HESSD
12, 12247–12280, 2015

Singh, S. K.: Ralte and volume of stream flow depletion due to unsteady pumping, J. Irrig. Drain. E.-Asce, 131, 539–545, 2005.
van der Spek, J. E., Bogaard, T. A., and Bakker, M.: Characterization of groundwater dynamics in landslides in varved clays, Hydrol. Earth Syst. Sc., 17, 2171–2183, 2013.
Wang, C. T. and Yeh, H. D.: Obtaining the steady-state drawdown solutions of constant-head and constant-flux tests, Hydrol. Process., 22, 3456–3461, 2008.
Yeh, H. D. and Chang, Y. C.: Recent advances in modeling of well hydraulics, Adv. Water Resour., 51, 27–51, 2013.
Yeh, H. D., Chang, Y. C., and Zlotnik, V. A.: Stream depletion rate and volume from groundwater pumping in wedge-shape aquifers, J. Hydrol., 349, 501–511, 2008.
Zlotnik, V. and Ledder, G.: Groundwater-flow in a compressible unconfined aquifer with uniform circular recharge, Water Resour. Res., 28, 1619–1630, 1992.
Zlotnik, V. and Ledder, G.: Groundwater velocity in an unconfined aquifer with rectangular areal recharge, Water Resour. Res., 29, 2827–2834, 1993.

HESSD
12, 12247–12280, 2015

Table 1. Classification of existing analytical solutions involving localized recharge.

References	Aquifer domain	Aquifer boundary conditions	Recharge		Remarks
			Region	Rate	
1-D groundwater flow					
Hantush (1963)	Infinite extent	None	Strip	Constant	
Rao and Sarma (1980)	Finite extent	Dirichlet	Strip	Constant	
Rao and Sarma (1984)	Finite extent	Dirichlet and no-flow	Strip	Constant	
Latinopoulos (1986)	Finite extent	Robin and Dirichlet/no-flow	Strip	Seasonal pulse	
Bansal and Das (2010)	Semi-infinite extent	Dirichlet	Strip	Constant	Sloping aquifer bottom
2-D groundwater flow					
Hantush (1967)	Infinite extent	None	Rectangle	Constant	
Manglik et al. (1997)	Rectangle	No-flow	Rectangle	Arbitrary function of time	
Manglik and Rai (1998)	Rectangle	Dirichlet	Rectangle	Arbitrary function of time	
Chang and Yeh (2007)	Rectangle	Dirichlet	Rectangle	Exponential decay	Sloping aquifer bottom
Bansal and Teloglou (2013)	Rectangle	Dirichlet at two adjacent sides and no-flow at the others	Rectangle	Exponential decay	Multiple recharges and pumping wells
3-D groundwater flow					
Dagan (1967)	Infinite extent	None	Rectangle	Constant	Laplace equation; approximate solution
Zlotnik and Ledder (1993)	Infinite extent	None	Rectangle	Constant	Laplace equation
Radial groundwater flow					
Zlotnik and Ledder (1992)	Infinite extent with finite thickness	None	Circle	Constant	First-order free surface equation
Rai et al. (1998)	Circle	Dirichlet	Circle	Exponential decay	
Ostendorf et al. (2007)	Infinite extent with finite thickness	None	Circle	Exponential decay	First-order free surface equation
Illas et al. (2008)	Circle	Dirichlet	Circle	Exponential decay	Leaky aquifer

HESSD
12, 12247–12280, 2015

Table 2. Default values of variables and hydraulic parameters used in the text.

Notation	Default value (unit)	Definition
h	None	Hydraulic head
(x, y, z)	None	Variables of Cartesian coordinate
t	None	Time
(K_x, K_y, K_z)	$(10, 10, 1\,\mathrm{m\,d^{-1}})$	Aquifer hydraulic conductivities in x, y, and z directions, respectively
(S_s, S_y)	$(10^{-5}\,\mathrm{m^{-1}}, 0.1)$	Specific storage and specific yield, respectively
I	$0.1\,\mathrm{m\,d^{-1}}$	Constant recharge rate
I_t	None	Transient recharge rate defined as $I_t(t) = I_1 + I_0\exp(-rt)$
$(I_1 + I_0, I_1)$	$(0.1, 0.05\,\mathrm{m\,d^{-1}})$	Initial and ultimate transient recharge rates, respectively
r	$10^3\mathrm{d^{-1}}$	Decay constant of transient recharge rate
(B,I,w)	(20 m, 1, 1 km)	Aquifer initial thickness and widths in x and y directions, respectively
d	50 m	Shortest distance between the edge of recharge region and an observation well
(x_1, y_1)	450 m	Location of bottom left corner of recharge region
(a, b)	100 m	Widths of recharge region in x and y directions, respectively
(K_1, K_2, K_3, K_4)	$0.1\,\mathrm{m\,d^{-1}}$	Hydraulic conductivities of media between aquifer and lateral boundaries 1, 2, 3 and 4, respectively
(b_1, b_2, b_3, b_4)	1 m	Widths of media between aquifer and lateral boundaries 1, 2, 3 and 4, respectively
(d_1, d_2, d_3, d_4)	450 m	Shortest distances from the edge of the region to lateral boundaries 1, 2, 3 and 4, respectively
R	None	$\min(d_1, d_2, d_3, d_4)$
$\overline{h}$	None	h/B
$\overline{R}$	None	R/d
$(\overline{x}, \overline{y}, \overline{z})$	(12, 10, −0.5)	$(x/d, y/d, z/B)$
$\overline{t}$	None	$K_x t/\left(S_s d^2\right)$
$(\kappa_y, \kappa_z, \varepsilon)$	(1, 0.625, 500)	$(K_y/K_x, K_z d^2/\left(K_x B^2\right), S_y/(S_s B))$
ξ	0.1	I/K_z
ξ_t	None	$\xi_1 + \xi_0\exp(-\gamma\overline{t})$
(ξ_1, ξ_0, γ)	(0.05, 0.05, 2.5)	$(I_1/K_z, I_0/K_z, rS_s d^2/K_x)$
$(\overline{l}, \overline{w}, \overline{a}, \overline{b})$	(20, 20, 2, 2)	$(l/d, w/d, a/d, b/d)$
$(\overline{x}_1, \overline{y}_1)$	9	$(x_1/d, y_1/d)$
$(\kappa_1, \kappa_2, \kappa_3, \kappa_4)$	0.5	$(K_1 d/(K_x b_1), K_2 d/(K_x b_2), K_3 d/(K_y b_3), K_4 d/(K_y b_4))$
$\left(\overline{d}_1, \overline{d}_2, \overline{d}_3, \overline{d}_4\right)$	9	$(d_1/d, d_2/d, d_3/d, d_4/d)$

HESSD
12, 12247–12280, 2015

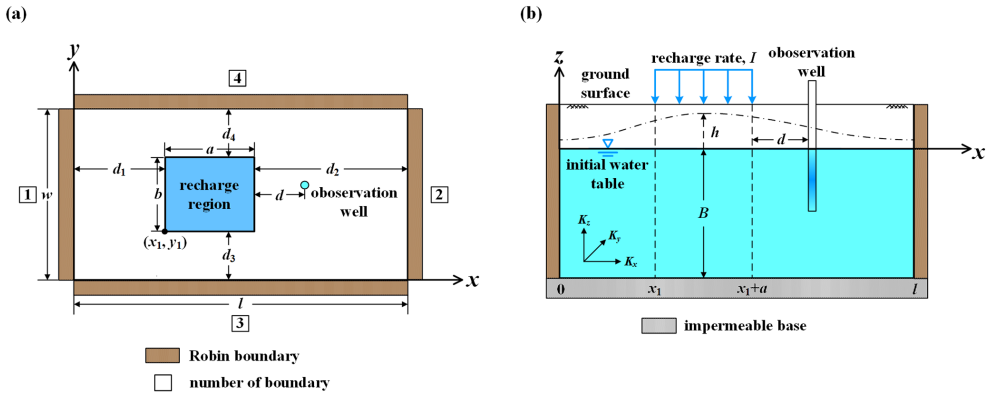

Figure 1. Schematic diagram of a rectangular-shaped unconfined aquifer with localized recharge **(a)** top view **(b)** cross section view.

HESSD
12, 12247–12280, 2015

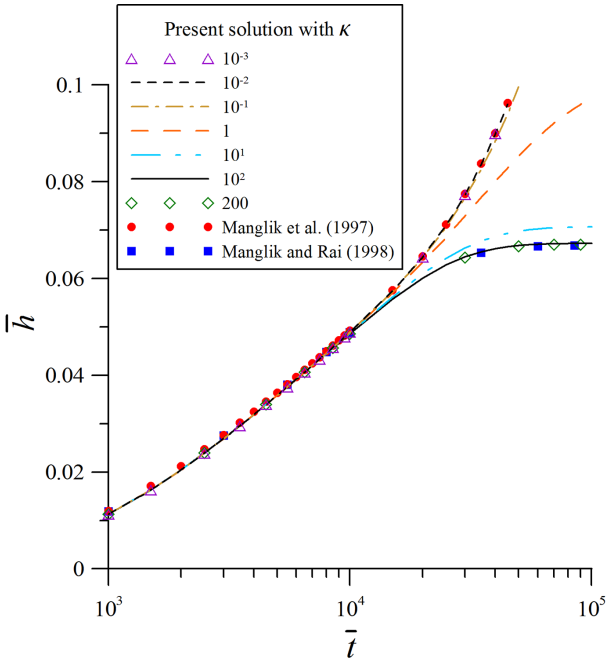

Figure 2. Temporal distributions of the dimensionless head predicted by Manglik et al. (1997) solution for a no-flow boundary, Manglik and Rai (1998) solution for a Dirichlet boundary, and the present solution with $\kappa_z = 1$ for a Robin boundary.

HESSD
12, 12247–12280, 2015

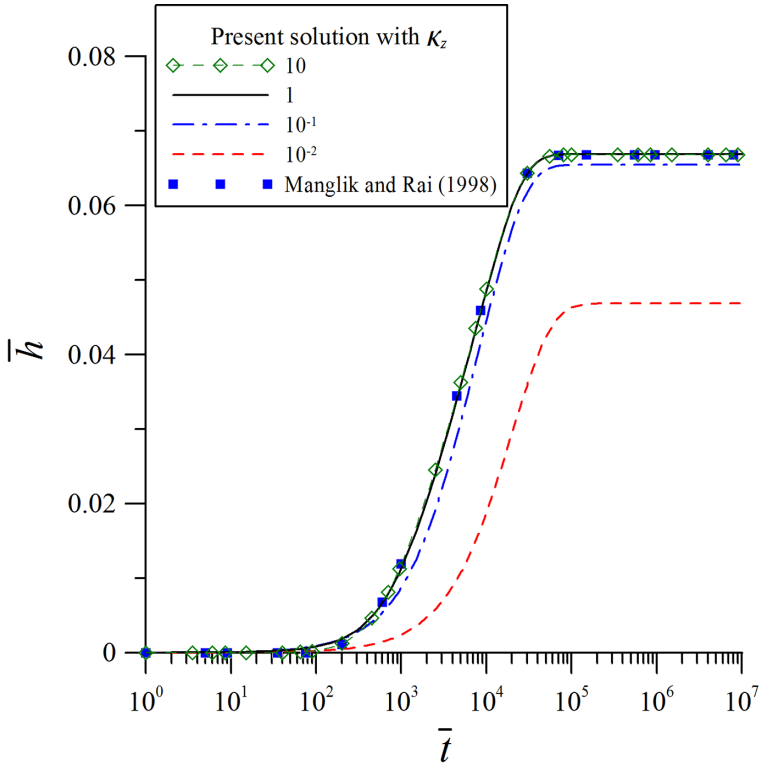

Figure 3. Temporal distributions of the dimensionless head predicted by Manglik and Rai (1998) solution based on 2-D flow and the present solution for 3-D flow with various κ_z.

HESSD
12, 12247–12280, 2015

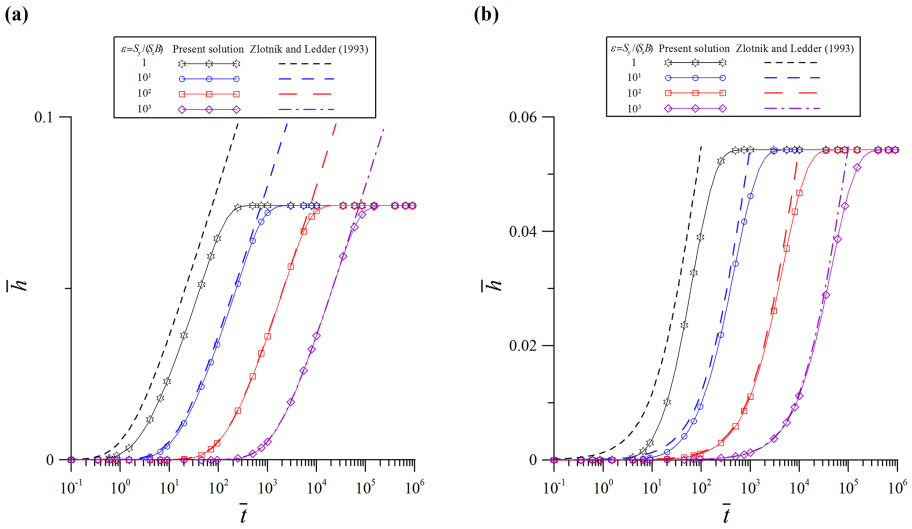

Figure 4. Temporal distributions of the dimensionless head for **(a)** $\kappa_z = 10^{-2}$ and **(b)** $\kappa_z = 10$ predicted by Zlotnik and Ledder (1993) solution based on the assumption of $S_s = 0$ and the present solution relaxing the assumption.

HESSD
12, 12247–12280, 2015

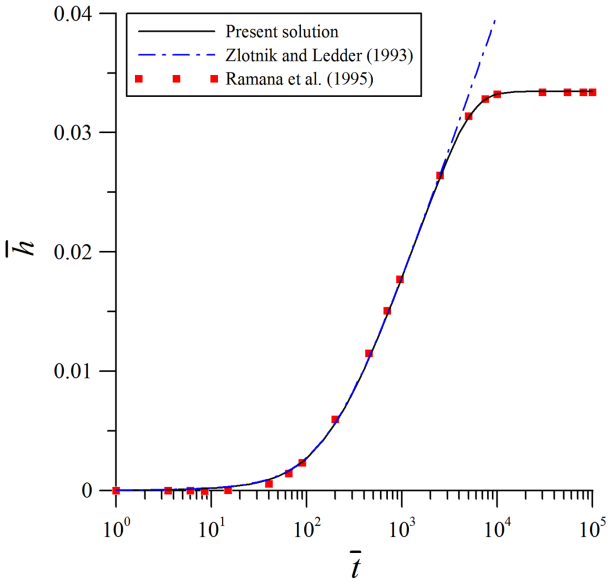

Figure 5. Temporal distributions of the dimensionless head subject to a transient recharge rate predicted by Ramana et al. (1995) solution, Zlotnik and Ledder (1993) solution, and the present solution with $\kappa_z = 1$, $\kappa = 100$, and $\varepsilon = 100$.

HESSD
12, 12247–12280, 2015

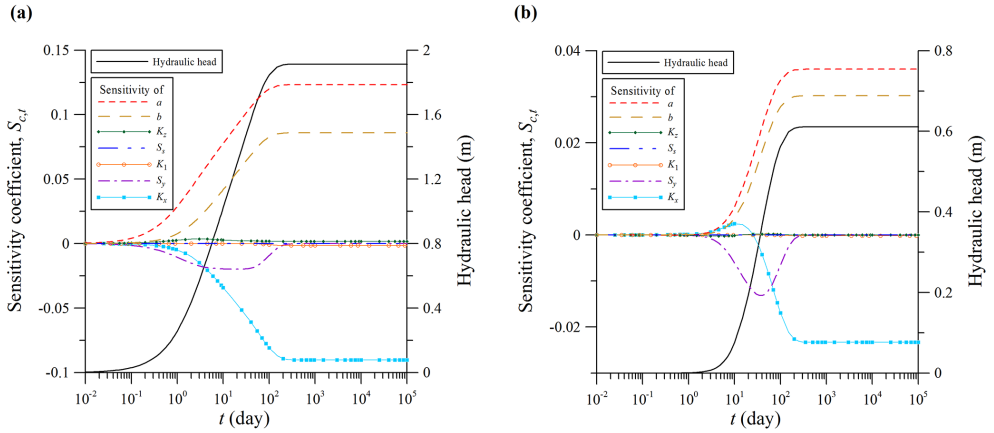

Figure 6. Temporal distributions of the normalized sensitivity coefficients of the hydraulic head at the observation points of **(a)** (x, y, z) = (555, 500, −10) and **(b)** (x, y, z) = (800, 500, −10) to the changes in parameters a, b, K_z, S_s, K_1, S_y, and K_x.

HESSD
12, 12247–12280, 2015